Reprint Series
7 May 1993, Volume 260, pp. 786–789

SCIENCE

A Photomicrodynamic System with a Mechanical Resonator Monolithically Integrated with Laser Diodes on Gallium Arsenide

Hiroo Ukita, Yuji Uenishi, and Hidenao Tanaka

Copyright © 1993 by the American Association for the Advancement of Science

A Photomicrodynamic System with a Mechanical Resonator Monolithically Integrated with Laser Diodes on Gallium Arsenide

Hiroo Ukita, Yuji Uenishi, Hidenao Tanaka

A cantilever resonant microbeam, laser diodes, and a photodiode have been fabricated on the surface of a gallium arsenide substrate. The microbeam is excited photothermally by light from a laser diode. The vibration is detected with a photodiode as the variation in light output caused by the difference in optical length between the microbeam and another laser diode. A high carrier-to-noise ratio (45 decibels) is achieved with a short (3 micrometers) external cavity length. Such a small distance allows a lensless system, which increases the ease of fabrication. This work could lead to applications in which photomicrodynamic systems are monolithically integrated on a gallium arsenide substrate with surface micromachining technology.

Established large-scale integration manufacturing techniques, such as photolithography, can be used for fabricating microstructures including resonant sensors, motors, valves, and pumps (*1–3*). Such microdevices have been made from silicon wafers, which have isodirectional etching properties. However, it has been impossible to integrate a light source with these Si-based micromechanical structures. Gallium arsenide (GaAs), on the other hand, is attractive for integrating optical and mechanical structures. The advantage of using an optical method is that it does not interfere electromagnetically. Furthermore, it could lead to developments in photomicrodynamics. With GaAs, not only would optical sensors and actuators be possible, but also micromechanical filters for optical signal processing and pickups for optical recording (*4, 5*).

A resonant sensor is a device that changes its mechanical resonant frequency as a function of a physical or chemical parameter, such as stress or mass-loading (*6*). Electrostatic (capacitive) excitation and detection or piezoelectric excitation and detection have been used for the conventional Si-based resonant sensors. The former method requires comparatively large electrode areas and small electrode distances (a few micrometers) if good signals are to be obtained. The latter requires a layer of a

NTT Interdisciplinary Research Laboratories, 9-11 Midori-cho 3-Chome, Musashino-shi, Tokyo 180, Japan.

piezoelectric material, preferably zinc oxide (ZnO). Unfortunately, however, ZnO is not compatible with integrated-circuit technology.

We have fabricated a resonant sensor on the surface of a GaAs substrate (Fig. 1) that uses optical excitation and detection. The cantilever microbeam is shaped by reactive dry-etching and undercut by selective wet-etching (the etching of AlGaAs is inhibited in highly Al-doped regions) so that it is free to vibrate. Light incident from laser diode LD2 on the side wall of the microbeam (MB) will be partially absorbed, heating the MB and producing the bending moment (*7*). The MB is excited by the thermal stress of the resonant frequency caused by a pulsed laser diode LD2.

This sideways vibration is detected by LD1 and photodiode PD from the variation in the external cavity length between the MB wall and the facet of LD1 (phase difference). The light incident from LD1 is continuous, and the amount of light is so small that it has no effect on the MB vibration. The light (wavelength $\lambda = 830$ nm) reflected from the MB wall interferes with the light from the facet of LD1. Maximum peaks in the light output occur every $\lambda/2$, and their amplitude decays exponentially in proportion to the external cavity length (*8*). The variation in light output caused by this vibration is detected as a signal by the PD.

The resonator was designed to optimize the efficiency of the photothermal excitation and the quality of the composite cavity signal with the structural configuration resulting from the fabrication process. We set the distance h_1 between the facet LD1 and the wall of the MB equal to 3.0 μm by considering the composite cavity signal-to-noise ratio and the aspect ratio h_1/w of the reactive dry-etching process. We set the distance h_2 between the facet of LD2 and the wall of the MB equal to 30 μm on the basis of the energizing light absorption on the MB and the hole size for the wet process described later. For the MB dimensions we used a length $\ell = 50$ or 110 μm, a thickness $t = 3$ μm, and a depth $w = 5$ μm, considering the resonant frequency of the MB. We determined the positions of the exciting light beam (LD2) and the detecting light beam (LD1) on the MB wall based on the consideration that the LD2 light strikes the MB closer to the support for better excitation and that the LD1 light strikes farther from the support for better detection and also to prevent "cross-talk" between the two light beams.

The short distance of the LD1-MB-LD2 structure is useful for a vibration resonator because no lenses are required in the structure to make the light beam converge, so it is easier to integrate the mechanical element with the optical elements. Furthermore, the integrated structure does not need any optical alignment like that required by conventional hybrid resonant sensors.

Three micromachining processes (Fig. 2) were carried out to fabricate a resonant MB integrated with two laser diodes: (i) An etch-stop layer of AlGaAs was formed in the laser diode structures prepared by metal organic vapor-phase epitaxy (Fig. 2A). (ii) The shape of the microstructure was precisely defined by means of a reactive dry-etching [reactive fast atom beam (*9*)] technique with chlorine, which can simultaneously form the vertical etched mirror facets for LDs (Fig. 2B). (iii) A wet-etch window was made with photoresist, and the microbeam was undercut by selective etching [sacrificial layer etching (*10*)] to leave the

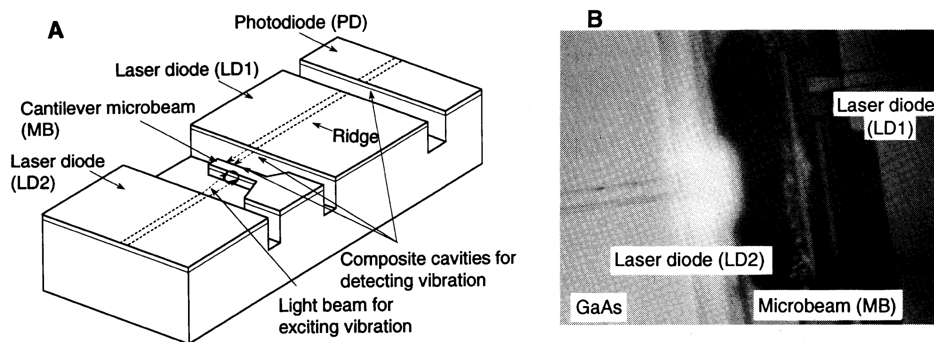

Fig. 1. (**A**) Structure and (**B**) photograph of a resonator sensor driven photothermally from one side (30 μm away) by laser diode LD2 and sensed optically from the other side (3 μm away) by laser diode LD1 and photodiode PD; LD1, LD2, and PD are integrated on a GaAs substrate by surface micromachining techniques.

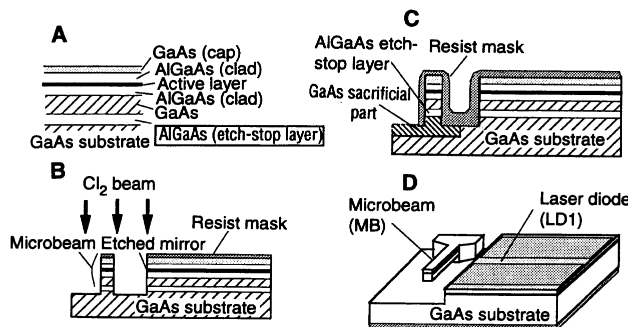

Fig. 2. Process steps used to fabricate a GaAs/AlGaAs resonant microbeam (MB) integrated with a laser diode (LD). (**A**) An AlGaAs etch-stop layer is introduced in the epitaxial growth. (**B**) The mechanical structure is defined by the shape of a mask and dry-etched by reactive fast atom beam etching with chlorine. (**C**) The mechanical structure is released from the GaAs substrate by wet-etching, which removes the sacrificial region. The bottom of the structure is protected by the etch-stop layer. The photoresist used to protect the top surface and side walls of the structure is removed by O_2 plasma etching. (**D**) Final structure of the integrated microbeam and laser diode.

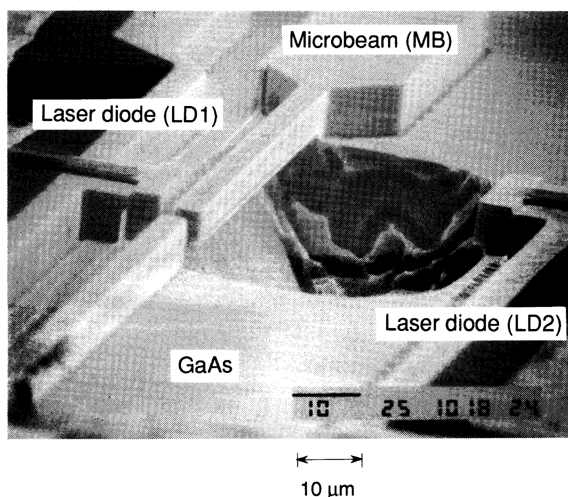

Fig. 3. Scanning electron microscope view of the main parts of the resonant sensor. We fabricated the released GaAs/AlGaAs microbeam (MB) by undercutting the sacrificial GaAs. The MB length, width, and thickness are 110, 3.0, and 5 μm, respectively, and the distances from the facet of LD1 to the side wall of the MB and LD2 to MB are 3.0 and 30 μm, respectively.

microbeam freely suspended (Fig. 2C). The final structure of the integrated microbeam and laser diode is shown in Fig. 2D.

Figure 3 shows a scanning electron microscope image of the main parts of the resonant sensor. The hole for wet-etching is visible under the microbeam between LD1 and LD2. On the basis of the size of the hole, the distance between the MB and LD2 was set to 30 μm. The shorter the MB-LD2 distance, the higher the photothermal conversion efficiency becomes. The threshold current of LD2 was 46 mA and that of LD1 was 64 mA (the threshold current of LD1 is higher because both of its mirrors were etched).

Table 1. Comparison of the mechanical and thermal properties of GaAs, Si, and steel.

Parameter	Material		
	GaAs	Si	Steel
ρ (g cm^{-2})	5.307	2.3	7.9
E (10^{12} dyne cm^{-2})	1.19	1.9	2.0
Thermal conductivity (W cm^{-1} K^{-1})	0.54	1.57	0.33
Thermal expansion (10^{-6} K)	6.0	2.5	17.3
Yield strength (10^{10} dyne cm^{-2})	4.0*	13*	0.8

*Single crystalline.

We used a function generator to drive LD2 with a sinusoidal signal to measure the resonant MB properties. When the frequency of the function generator coincided with the MB mechanical resonant frequency, the amplitude of the PD signal exhibited a maximum. Figure 4 shows the output amplitude signals and resonant frequency spectra for a 110-μm-long microbeam. The signal-to-noise ratio is high (45 dB) because of the lack of mode hop noise owing to the extremely short (3 μm) external cavity signal. The signal amplitude increases as the LD2 light power increases, but an inversion appears in the signal peak for light power over 30 mW because the vibration amplitude is larger than $\lambda/4$. We can measure the absolute amplitude from the fact that the peak signal amplitude corresponds to $\lambda/4$ (0.21 μm). As the incident light power rises, producing greater thermal expansion (stress) in the microbeam, the vibration amplitude increases. The resonances of the microbeam for lengths of 110 and 50 μm are 200.6 kHz and 1.006 MHz, respectively. The mechanical quality (Q) values in air are ~250. If the Q values are to be increased, damping mechanisms such as imbalance and radiation at the supporting rim will require further study.

Figure 5 shows the resonance frequency as a function of microbeam (cantilever) length for GaAs and Si. The circles and triangles are experimental measurements for GaAs and Si, respectively (*11*), and they are in good agreement with the theoretical results (*12*) calculated from Eq. 1 using the parameter values listed in Table 1

$$f_0 = \lambda_0^2 t (E/12\rho)^{1/2}/2\pi\ell^2 \quad (1)$$

where λ_0 is the eigen value of 1.875 determined by the vibration mode, E is Young's modulus, ρ is the density, ℓ is the cantilever length, and t is its thickness. To increase the sensor sensitivity, the resonant frequency should be raised by shortening the cantilever length. A resonant frequency of 10 MHz is available with a length of less than 20 μm (3 μm thick), if Eq. 1 is valid for a beam of micrometer-scale length. The physical properties of a microstructure usually differ somewhat from bulk values (*13*), but the bulk parameters can indicate relative trends in the micromechanical properties of the materials.

Monolithic structures that integrate a mechanical element, such as a resonant MB, with optical elements, such as an LD and a PD, on a single GaAs substrate promise many applications. These include resonant frequency change-detection sensors such as accelerometers for control systems and mechanical filters that would syncronize signal detection in communication systems. The yield strength of single crystalline GaAs is less than that of Si (see Table 1), but it is five times that of steel. Furthermore, surface micromachining can be used to fabricate microstructures of high purity with a low defect density and no residual stress. These mechanical properties make GaAs-based microstructures suitable for integrated photomicrodynamic systems. This technology could have a significant effect on engineering design and interdisciplinary activity.

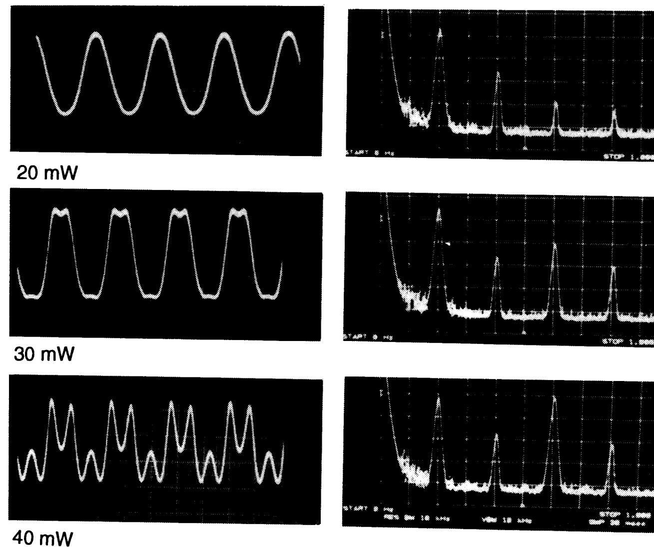

Fig. 4. Variations in MB vibration amplitude and its frequency spectrum as a function of excitation light power; f_0 = 200.6 kHz, ℓ = 110 μm, t = 3 μm, and w = 5 μm.

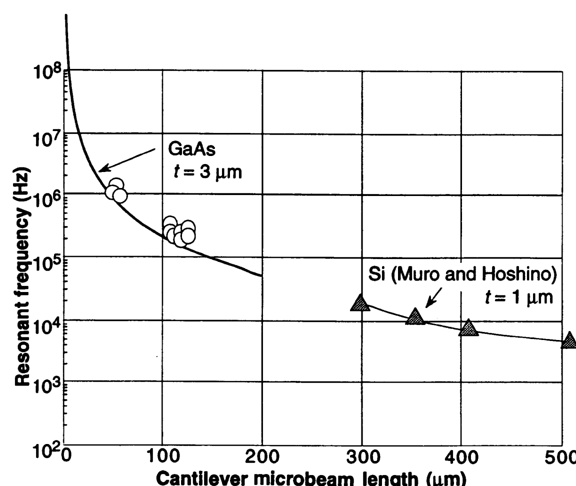

Fig. 5. Resonance frequency as a function of cantilever microbeam length for GaAs and Si. The solid lines are theoretical results; the circles and triangles are experimental measurements for GaAs and Si, respectively (*11*).

REFERENCES AND NOTES

1. K. E. Drexler, *Engines of Creation* (Anchor Books, Doubleday, New York, 1987), p. 3.
2. R. S. Muller, *Sensors Actuators* **A21–23**, 1 (1990).
3. K. D. Wise and K. Najafi, *Science* **254**, 1335 (1991).
4. H. Ukita, Y. Katagiri, S. Fujimori, *Appl. Opt.* **28**, 4360 (1989).

5. J.-Y. Kim and H. C. Hseih, *J. Lightwave Technol.* **10**, 439 (1992).
6. G. Stemme, *J. Micromech. Microeng.* 1, 113 (1991).
7. K. Hane and S. Hattori, *Appl. Opt.* **29**, 145 (1990).
8. H. Ukita, Y. Katagiri, Y. Uenishi, *Jpn. J. Appl. Phys.* **26** (suppl. 26-4), 111 (1987).
9. F. Shimokawa, H. Tanaka, Y. Uenishi, R. Sawada, *J. Appl. Phys.* **66**, 2613 (1989).
10. Z. L. Zhang, G. A. Porkolab, N. C. MacDonald, in *Proceedings of IEEE Micro Electro Mechanical System '92*, W. Benecke and H.-C. Petzold, Eds. (Travemünde, Germany, 4 to 7 February 1992) (IEEE, New York, 1992), p. 72.
11. H. Muro and S. Hoshino, *Trans. Inst. Electron. Inf. Commun. Eng.* **J74-C-II**, 421 (1991) (in Japanese).
12. M. Tabib-Azar and J. S. Leave, *Sensors Actuators*, **A21–23**, 229 (1990).
13. D. Walsh and B. Culshaw, *ibid.* **A25–27**, 711 (1991).
14. We thank K. Itao and E. S. Vera for helpful discussions.

29 September 1992; accepted 2 February 1993